2010 American Control Conference
Marriott Waterfront, Baltimore, MD, USA
June 30-July 02, 2010

Modeling and Control of Cyclic Systems in Xerography

ShiNung Ching, Yongsoon Eun, Eric Gross, Eric Hamby, Pierre Kabamba, Semyon Meerkov and Amor Menezes

***Abstract*— This paper is devoted to the scientific study and engineering application of *cyclic systems*. Cyclic systems are non-traditional plants, containing devices with rotating dynamics along with actuators and sensors fixed in inertial space. The combination of rotating dynamics and inertially-fixed inputs and outputs leads to one-per-revolution (or *stroboscopic*) actuation and sensing. Control of cyclic systems amounts to designing a regulator that uses stroboscopic actuation and sensing to force the system into the desired regime. Although cyclic systems are periodic, the general theory of periodic control is not immediately applicable due to stroboscopic actuation and sensing. Because of rotating dynamics, the theory of impulsive control is not applicable as well. This work develops an approach to the control of systems with both rotating dynamics and stroboscopic instrumentation, and reports the initial application to a xerographic process.**

I. INTRODUCTION

XEROGRAPHY is the dry ink marking process employed by photocopying machines and printers. A photoconducting drum or belt, called the *photoreceptor*, is at the heart of this process. To produce a document image, the photoreceptor undergoes five stages per revolution (see Fig. 1):

1) *Charging*, where the photoreceptor is charged to a voltage.
2) *Exposing*, where a laser electrostatically writes the latent image on the photoreceptor surface.
3) *Developing*, where the toner particles are deposited on the written image.
4) *Transferring*, where the toner particles are transferred from the photoreceptor to paper.
5) *Cleaning and erasing*, where the photoreceptor is mechanically cleaned of toner residue and electrostatically discharged.

At times, xerographic images exhibit defects such as banding (lines in the cross-process direction), streaking (lines in the process direction), and ghosting (prior image retention). These defects have been often attributed to the photoreceptor. More specifically, photoreceptor-induced defects are caused by variation in photoreceptor thickness, aging charger, and imperfect electrostatic erase that leaves residual voltage on the photoreceptor surface. Ensuring a uniform photoreceptor surface voltage will reduce the impact that these factors have on print quality. The traditional approach to address the non-uniformity of the surface voltage is to employ better hardware. The approach in this paper is to employ feedback control to ensure that the surface voltage is uniform. (Note that feedback control to alleviate banding has been used in the past, e.g., [1], using drive motor speed modulation.)

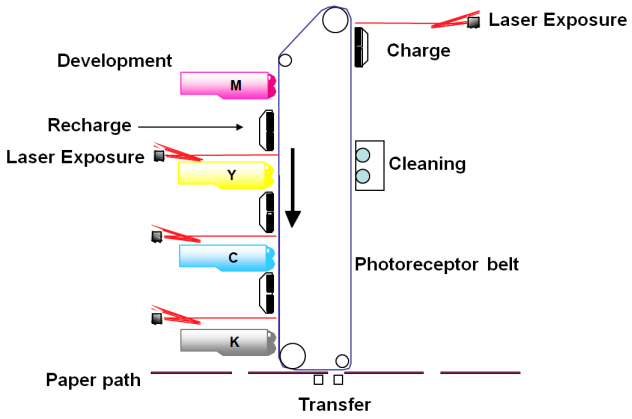

Fig. 1. The photoreceptor system in a xerographic process.

The photoreceptor system is an example of a *cyclic system*. Cyclic systems are a non-traditional class of plants, containing devices with rotating dynamics, along with actuators and sensors that are fixed in inertial space. The combination of rotating dynamics and inertially-fixed inputs and outputs leads to a property called *stroboscopicity*. Stroboscopicity refers to the one-per-revolution actuation and sensing of a portion of the rotating device, whenever this portion is located at either the actuator or the sensor. Thus, inertially-fixed inputs and outputs result in actuation and sensing that are similar to a stroboscope. In xerography, portions of the rotating photoreceptor are charged (i.e., actuated), exposed, developed, transferred, erased and cleaned, and electrostatically and optically measured (i.e., sensed) once per revolution, whenever the portion passes under the devices corresponding to the actuations and sensing [2]. Thus, to guarantee the desired performance of the photoreceptor as a cyclic system, a controller employing stroboscopic sensing and actuation must be designed.

Cyclic systems arise naturally in other subsystems of the xerographic process and in other practical applications as well. These include:

- The *toner replenishment* stage of the xerographic process, which requires that toner mass be transferred

S. Ching is with the Massachusetts Institute of Technology, Cambridge, MA 02139, USA shinung@mit.edu

Y. Eun, E. Gross and E. Hamby are with the Xerox Research Center, Webster, NY 14580, USA Yongsoon.Eun@xerox.com; Eric.Gross@xerox.com; Eric.Hamby@xerox.com

P. Kabamba, S. Meerkov and A. Menezes are with the University of Michigan, Ann Arbor, MI 48109, USA kabamba@umich.edu; smm@umich.edu; amenezes@umich.edu

onto a rotating roll prior to image development on the photoreceptor. The quantity of toner mass on the surface of the roll may be sensed stroboscopically, and the requisite mass transfer takes place stroboscopically as well [3]. Hence, the roll is a cyclic system. The *fuser* in the xerographic process is also cyclic — the temperature of the rotating fuser is measured stroboscopically, and heat is applied in a stroboscopic manner [4].

- Printing press processes are similar to the xerographic toner and fuser heat control processes described above.
- Drilling and milling machines can also be viewed as cyclic systems. Similarly, a turbomachine, where each rotating blade in a turbofan engine encounters fast-moving air, is a cyclic system too.

The amount of variation of a field variable (charge, voltage, mass, heat etc.) over the surface of the rotating device is often employed as a performance metric for the cyclic system. For instance, during the exposure stage of the xerographic process, uniformity of the photoreceptor surface charge in both circumferential and axial directions is desired. Likewise, in the toner replenishment stage, the uniform distribution of toner mass along the surface of the roll must be guaranteed because inconsistent toner mass distribution results in images with varying contrast. Finally, during the fusing stage, a uniform temperature along the surface of the fuser is required to enable the even appearance of the image on paper. Similar performance metrics can be formulated for the other applications mentioned above. These performance metrics may be used to evaluate and compare the efficacy of traditional hardware-based approaches to novel feedback-control approaches.

Accordingly, the goals of this paper are:

- The mathematical modeling of cyclic systems taking into account the device's rotating dynamics as well as stroboscopic actuation and sensing.
- Stability and controllability analysis of cyclic systems.
- Controller design.
- The application and verification of the results via simulations using experimental data.

Although there is a vast body of literature on periodic control systems (see [5] and references therein), cyclic systems form a specific category of such systems because of the stroboscopic nature of actuation and sensing. The stroboscopicity of control is similar to that of impulsive control systems [6]. However, cyclic systems include devices with rotating dynamics, and these types of plants have not been investigated in the traditional impulsive control literature. This paper presents initial results on the control of systems with rotating dynamics and stroboscopic instrumentation.

The remainder of this work is organized as follows: Section II discusses the modeling and control of cyclic systems, focusing on the properties of stabilizability and disturbance rejection. Section III illustrates the application of the approach to a xerographic system, presenting the results of experiments and controller design. For proprietary reasons, all data have been represented with symbols.

II. MODELING AND CONTROL OF CYCLIC SYSTEMS

A. Modeling

The mathematical model of a cyclic system is generally infinite-dimensional. Such a model, while analytically feasible, is not always computationally tractable. A lumped parameter approach to modeling is therefore necessary, where the surface of the rotating device is divided into N discrete wedges (see Fig. 2). Thus, describing the field variable of the rotating device reduces to describing the average value of the field variable on a wedge.

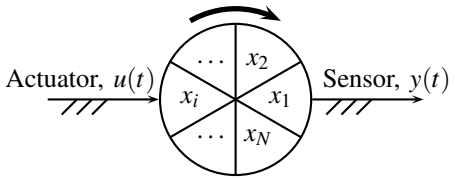

Fig. 2. Lumped model of a rotating device in a cyclic system.

We model the stroboscopic actuators and sensors by defining a stroboscope function as follows:

$$\mathrm{str}_i(t) = \begin{cases} 1, & t \in [\tau(Nk+i-1), \tau(Nk+i)), \\ 0, & \text{otherwise}, \end{cases} \qquad i = 1,2,\ldots,N;\ k = 0,1,\ldots, \tag{1}$$

where τ is the duration of the strobe and k is the rotation number. Hence, $\mathrm{str}_i(t)$ is zero except when the i^{th} wedge is actuated or sensed.

For simplicity, assume that the field variable on each wedge has first order dynamics. Since each wedge interacts circularly with the other wedges of the rotating device, the resulting scalar equations are

$$\dot{x}_1(t) = a_1 x_1(t) + a_2 x_2(t) + \ldots + a_N x_N(t) + bu(t) \cdot \mathrm{str}_1(t), \tag{2}$$

$$\dot{x}_2(t) = a_N x_1(t) + a_1 x_2(t) + \ldots + a_{N-1} x_N(t) + bu(t) \cdot \mathrm{str}_2(t), \tag{3}$$

$$\cdots$$

$$\dot{x}_N(t) = a_2 x_1(t) + \ldots + a_N x_{N-1}(t) + a_1 x_N(t) + bu(t) \cdot \mathrm{str}_N(t), \tag{4}$$

$$y(t) = \sum_{i=1}^{N} c x_i(t) \cdot \mathrm{str}_{(i+J_s) \bmod N}(t), \tag{5}$$

where x_i, $1 \le i \le N$, is the state of the i^{th} wedge, i.e., the value of the field variable on that wedge; a_1 is the inverse of the time constant of the decay of the field variable in a wedge; a_j, $2 \le j \le N$, represents the interaction between the field variable in a wedge and the field variable in the wedge $j-1$ wedges behind; b is the actuator gain; c is the sensor gain, $u(t)$ is the actuator input; $y(t)$ is the sensor output; and J_s is the number of wedges that the sensor is offset from the

actuator. If $J_s = 0$, the actuator and sensor are *collocated*; otherwise, they are *non-collocated*. Non-collocation is more typical than collocation due to physical constraints on the placement of actuators and sensors.

From (2)-(4), the plant matrix of this cyclic system is

$$A = \begin{bmatrix} a_1 & a_2 & \dots & a_N \\ a_N & a_1 & \dots & a_{N-1} \\ \vdots & \vdots & \ddots & \vdots \\ a_2 & \dots & a_N & a_1 \end{bmatrix}. \quad (6)$$

Matrices of this form are called *circulant* because each row is a circular permutation of the previous row. Hence, the circular wedge-to-wedge interactions in the physical model of a cyclic system induces circulancy in the mathematical model of the dynamics of the cyclic system.

Circulant matrices possess important properties; specifically, they form a commutative algebra. Moreover, the following three properties [7] are significant for the stability analysis of the systems at hand.

1) Let W be the trivial circulant matrix,

$$W := \begin{bmatrix} 0 & 1 & 0 & \dots & 0 \\ 0 & 0 & 1 & \dots & 0 \\ \vdots & \vdots & \vdots & \ddots & \vdots \\ 1 & 0 & 0 & \dots & 0 \end{bmatrix}. \quad (7)$$

Then any circulant matrix (6) can be represented as a linear combination of powers of W, i.e.,

$$A = f(W) = a_1 W^0 + a_2 W^1 + \ldots + a_N W^{N-1}. \quad (8)$$

2) The eigenvalues of the matrix W, w_1, w_2, …, w_N, are the N^{th} roots of 1. The eigenvalues of the circulant matrix A are given by $f(w_i)$, $1 \le i \le N$, where $f(\cdot)$ is defined in (8).
3) The circulant matrix A in (6) is Hurwitz if and only if the coefficients a_1, a_2, …, a_N satisfy the following N *linear* inequalities:

$$Re(a_1 + a_2 w_i + \ldots + a_N w_i^{N-1}) < 0, \ 1 \le i \le N. \quad (9)$$

Thus, stability analysis of the lumped parameter model of a cyclic system amounts to verifying the set of linear inequalities (9), rather than nonlinear inequalities arising from the Routh-Hurwitz criterion.

B. Stabilizability

For the sake of clarity, the remainder of this section uses an N-wedge model of a cyclic system that omits wedge interactions. There is a strong rationale for this assumption: wedge interactions in xerographic processes have been experimentally verified to be weak.

Under this assumption, the system equations (2)-(5) become:

$$\dot{x}_1(t) = a_1 x_1(t) + (b \cdot \mathrm{str}_1(t))\, u(t), \quad (10)$$

$$\dots$$

$$\dot{x}_N(t) = a_1 x_N(t) + (b \cdot \mathrm{str}_N(t))\, u(t), \quad (11)$$

$$y(t) = (c \cdot \mathrm{str}_{1+J_s}(t)) x_1(t) + \ldots + (c \cdot \mathrm{str}_{N+J_s}(t)) x_N(t). \quad (12)$$

Assuming that no disturbance affects any wedge between the instants of actuation and sensing, and recognizing that instantaneous feedback $u(t) = -Ky(t)$ will have limited stabilizing capability in the non-collocated case, we use the *time-delayed* output feedback,

$$u(t) = -Ky(t - J_s\tau), \quad (13)$$

where $0 \le J_s \le N-1$. With this feedback, we obtain the following closed loop equations:

$$\dot{x}_1(t) = (a_1 - bKc \cdot \mathrm{str}_1(t)) x_1(t), \quad (14)$$

$$\dots$$

$$\dot{x}_N(t) = (a_1 - bKc \cdot \mathrm{str}_N(t)) x_N(t), \quad (15)$$

which imply that the closed loop system is periodic.

A straight-forward calculation yields the following monodromy matrix, M, the state transition matrix over the period:

$$M = \begin{bmatrix} e^{(Na_1 - bKc)\tau} & 0 & \dots & 0 \\ 0 & e^{(Na_1 - bKc)\tau} & \dots & 0 \\ \vdots & \vdots & \ddots & \vdots \\ 0 & 0 & \dots & e^{(Na_1 - bKc)\tau} \end{bmatrix}. \quad (16)$$

Therefore, a necessary and sufficient condition for the stability of (14)-(15) is

$$\max_i |\lambda_i| < 1, \quad (17)$$

where λ_i denotes the i^{th} eigenvalue of M. This implies that the cyclic feedback ensures asymptotic stability if and only if

$$K > \frac{Na_1}{bc}. \quad (18)$$

Hence, with time-delayed output feedback, the cyclic system with no wedge interactions is stabilizable by output feedback. Note that it is not stabilizable by instantaneous output feedback.

In the general case of N interacting wedges, it can be shown that the monodromy matrix is similar to a circulant matrix. This implies that stabilizability can be analyzed using properties 1)-3) of Subsection II-A.

C. Disturbance Rejection

Time-delayed output feedback also enables the rejection of disturbances at the input of the actuator. Modifying the cyclic system (10)-(12) to include these disturbances yields the following equations:

$$\dot{x}_1(t) = a_1 x_1(t) + (b \cdot \mathrm{str}_1(t))\, u(t) + (e \cdot \mathrm{str}_1(t))\, d(t), \quad (19)$$

$$\dots$$

$$\dot{x}_N(t) = a_1 x_N(t) + (b \cdot \mathrm{str}_N(t))\, u(t) + (e \cdot \mathrm{str}_N(t))\, d(t), \quad (20)$$

$$y(t) = (c \cdot \mathrm{str}_{1+J_s}(t)) x_1(t) + \ldots + (c \cdot \mathrm{str}_{N+J_s}(t)) x_N(t), \quad (21)$$

where $e \cdot d(t)$ is the disturbance.

During each actuation interval, we wish to minimize the effect of the disturbance at the output while ensuring stability. That is, we consider the optimization problem

$$\min_K \left\| G_{dy}(s) \right\|_2^2, \tag{22}$$

$$\text{subject to } K > \frac{Na_1}{bc}, \tag{23}$$

where $G_{dy}(s)$ is defined as

$$G_{dy}(s) := \frac{ce}{s - a_1 + bKc}. \tag{24}$$

In other words, the optimization problem (22)-(23) is

$$\min_K \left\| G_{dy}(s) \right\|_2^2 = \min_K \frac{c^2 e^2}{2\left(a_1 - bKc\right)^2}, \tag{25}$$

$$\text{subject to } K > \frac{Na_1}{bc}. \tag{26}$$

Clearly, this problem has no solution, but the cost function can be made arbitrarily small by selecting K sufficiently high. Therefore, in cyclic systems with no wedge interactions, it is possible to reject disturbances to any desired level using time-delayed output feedback with sufficiently large gain K.

The results of this section indicate that stroboscopicity in actuation and sensing do not diminish the efficacy of feedback control in the case of no wedge interactions.

III. APPLICATION TO XEROGRAPHY

A. Experimental Modeling of the Photoreceptor as a Cyclic System

A number of experiments were conducted at the Xerox Research Center in Webster, New York on a physical system that exhibited all of the cyclic features described above. This system was also representative of the technology used in most current xerographic products. To facilitate the experiments, the machine was instrumented with sensors and actuators that are not found in the off-the-shelf product. In particular, an electrostatic voltmeter (ESV) and an optical toner mass sensor (OTMS) were used to measure the voltage and toner mass density on the surface of the photoreceptor, respectively. In addition, an optical scanner was used to measure the print uniformity on the output page.

The first set of experiments focused on model development through system identification. This involved applying various signals at the input (the charger) and measuring the output at different locations (the ESV, the OTMS and the printed page). Signals used included sinusoids and pseudo-random binary noise. The results gave information on the dynamic behavior of the photoreceptor, and thus helped determine the model structure and parameters. Specifically, the experiments helped identify the following:

- The inverse of the time constant of a single wedge, i.e., a_1 in (10)-(11).
- The absence of coupling between wedges.
- The size of the wedge to achieve the performance requirement, or equivalently, the number of wedges, N, in (10)-(11).

The second series of experiments studied the sources of disturbance that affect the photoreceptor, and how they manifest at the output, i.e., the print quality. A test was carried out in which one hundred sheets of a halftone image were printed. In perfect conditions, this type of print job would produce completely uniform voltage on the surface of the photoreceptor, uniform toner mass density, and a uniform visual image on the printed page. This experiment produced two important conclusions.

1) Variations in the surface voltage are highly correlated with variations in toner mass, and subsequently, with uniformity on the printed page.
2) Many distinct noise sources contribute to variations in surface voltage.

The first conclusion is important since it confirms that fluctuations in the surface voltage are responsible for defects in the output print. The second conclusion helps refine the model by clarifying which disturbances cause these fluctuations. In particular, we obtained the spatial spectrum of the output print, shown in Fig. 3. This figure depicts three significant peaks at low frequency. Other than the peak at ω_m, which is likely caused by the toner transfer mechanical system, the dominant frequency components occur at ω_{pr} and ω_c, which correspond to the periods of rotation of the photoreceptor and charger, respectively. Hence, it is determined that parametric variation along the surface of the photoreceptor is the primary source of voltage fluctuation.

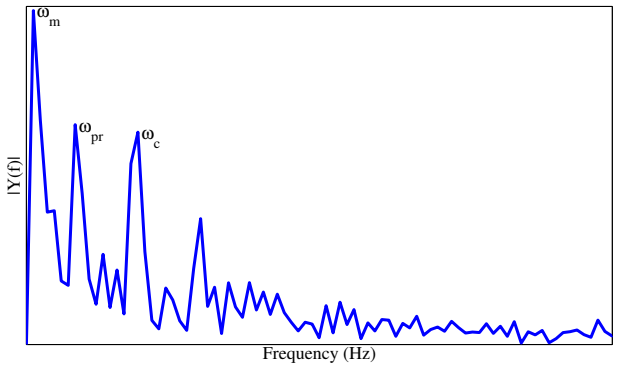

Fig. 3. Spectrum of the output print.

Accordingly, a mathematical model of the photoreceptor cyclic system was formulated, with the goal of duplicating the experimental observations. This model includes two key features:

1) To simulate the photoreceptor voltage, the effect of erase is taken into account explicitly while the effects of all other stages are modeled as a disturbance.
2) To account for the fact that charging occurs only if the voltage difference between the charger and photoreceptor is above a certain threshold, a deadzone nonlinearity is used.

As a result, we obtain the following model:

$$\begin{cases} \dot{x}_i(t) = a_1 x_i(t) + b_i v_i(t) \cdot \mathrm{str}_i(t) + f(t) \cdot \mathrm{str}_{(i+J_e) \bmod N}(t), \\ \qquad t \in [\tau(Nk+i-1), \tau(N(k+1)+i-1)), \\ \\ x_i(\tau(Nk+i-1)) = V_{res_i}, \end{cases} \tag{27}$$

for $k = 0,1,2,\ldots; 1 \le i \le N$, with

$$y(t) = \sum_{i=1}^{N} x_i(t) \cdot \mathrm{str}_{(i+J_s) \bmod N}(t) + \varepsilon(t). \tag{28}$$

The first equation in (27) describes the behavior of the voltage of the i^{th} wedge, while the second models the erase, where V_{res_i} is the residual voltage of the i^{th} wedge after the erase stage. In (27), $f(t)$ is intended to represent the effects of expose, develop and transfer on the photoreceptor, while $v_i(t)$ is the charging (control) input accounting for the deadzone nonlinearity, defined by

$$v_i(t) = \gamma(DZ_i(u_i(t) - x_i(t))), \ \gamma > 0, \tag{29}$$

where $u_i(t)$ is the voltage applied by the charger to the i^{th} wedge and DZ_i is the deadzone function of the i^{th} wedge, given by

$$DZ_i(u_i(t) - x_i(t)) = \begin{cases} \alpha(u_i(t) - x_i(t) - \frac{\delta_i}{2}), \\ \quad u_i(t) - x_i(t) \ge \frac{\delta_i}{2}, \ \alpha > 0, \\ 0, \frac{-\delta_i}{2} < u_i(t) - x_i(t) < \frac{\delta_i}{2}, \\ \alpha(u_i(t) - x_i(t) + \frac{\delta_i}{2}), \\ \quad u_i(t) - x_i(t) \le \frac{-\delta_i}{2}, \ \alpha > 0. \end{cases} \tag{30}$$

In (30), δ_i and α are the parameters of the nonlinearity. Finally, (28) models the reading of the ESV where $\varepsilon(t)$ is measurement noise.

Note that the width of the deadzone, δ_i, differs from wedge to wedge, and is the primary source of variation in voltage along the surface of the photoreceptor. The variability in the deadzone width results from nonuniformity in the thickness of the photoreceptor, which in turn leads to variation in the electric field generated by the charger.

The specific parameters in (27)-(30) are identified through experimentation and physical knowledge of the system. In particular, the single-wedge parameters a_1 and b_i are obtained through classical system identification techniques. The parameters τ, J_e and J_s are obtained from physical measurements. The deadzone width nonuniformity is modeled by observing that the surface of the photoreceptor exhibits voltage variation of $\pm\Delta_{var}$.

B. Disturbance Rejection Controller and Its Verification

Using the model (27)-(30) with, for simplicity, $N = 3$, the performance of the photoreceptor has been analyzed numerically in four scenarios:

1) Open loop with perfect erase, i.e., with $u_i(t)$ = constant, and $V_{res_i} = 0$.
2) Closed loop using cyclic feedback, assuming perfect knowledge of the photoreceptor parameters and perfect erase, i.e., with $a_1 = a_{nom}$ and $V_{res_i} = 0$. The cyclic feedback in this and the two subsequent scenarios is given by

$$u_i(t) = u_i(t - N\tau) + V_{nom} - y((N(k-1) + J_s + i - 1)\tau), \tag{31}$$

where $t \in [Nk\tau, \ N(k+1)\tau), \ k = 1,2,\ldots$.
3) Closed loop using cyclic feedback, assuming perfect knowledge of the photoreceptor parameters, but imperfect (random) erase, i.e., with V_{res_i} distributed uniformly on the interval $[-V^*_{res}, V^*_{res}]$.
4) Closed loop using cyclic feedback, assuming imperfect knowledge of the photoreceptor parameters and perfect erase, i.e., with $V_{res_i} = 0$ and $a_1 = 1.5 a_{nom}$.

The results are shown in Figs. 4-7, respectively. In these figures, the top portion shows the time history of the surface voltage of each wedge, x_i, over five revolutions of the photoreceptor, while the bottom portion shows the sampled time history of the measurement, y. In both portions of these figures, the experimentally measured voltage variation $\pm\Delta_{var}$ around the target voltage V_{nom} is indicated by dotted lines. In the top portion of each figure, the surface voltage of each wedge undergoes three stages per revolution: a charge to a negative target voltage V_{nom}, an electrostatic discharge during which the measurement is taken, and a reset to the target charge of V_{res}.

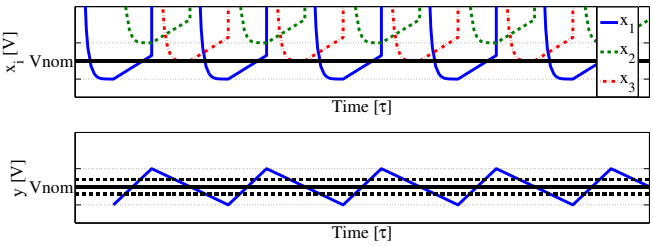

Fig. 4. Behavior of the photoreceptor in Scenario 1.

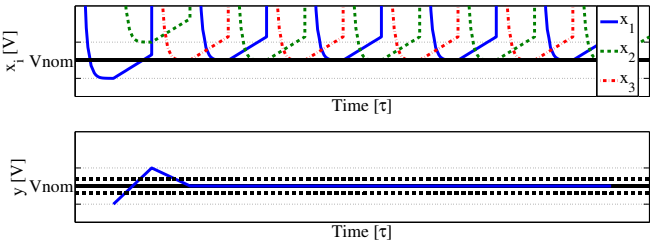

Fig. 5. Behavior of the photoreceptor in Scenario 2.

The performance specification for the controller design is to reduce the voltage variation around its steady-state value from $\pm\Delta_{var}$ to $\pm\Delta_{des}$, where $\Delta_{des} < \Delta_{var}$. In the bottom portion of Figs. 4-7, the acceptable voltage variation interval around the steady-state voltage is indicated by dashed lines, while the behavior of the output $y(t)$ is indicated by the thick curve.

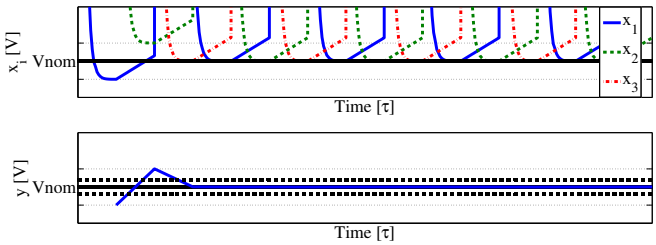

Fig. 6. Behavior of the photoreceptor in Scenario 3.

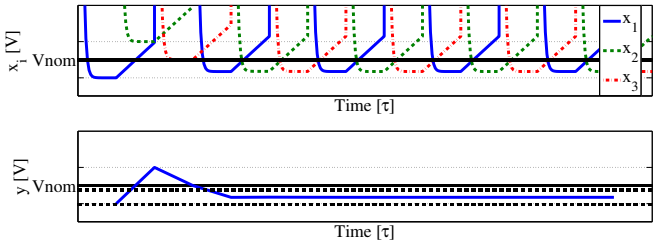

Fig. 7. Behavior of the photoreceptor in Scenario 4.

A comparison of Figs. 4 and 5 indicates that the cyclic control law (31) meets the controller design specification assuming perfect knowledge of wedge dynamics and perfect erase.

To assess the robustness of the controller (31) with respect to imperfect erase, assume that, in Scenario 3 above, the wedges are randomly reset, yielding a sample time history of wedge voltages shown in Fig. 8. In this scenario, the performance of the controller is illustrated in Fig. 6, which shows that the controller is capable of rejecting the disturbance caused by imperfect erase.

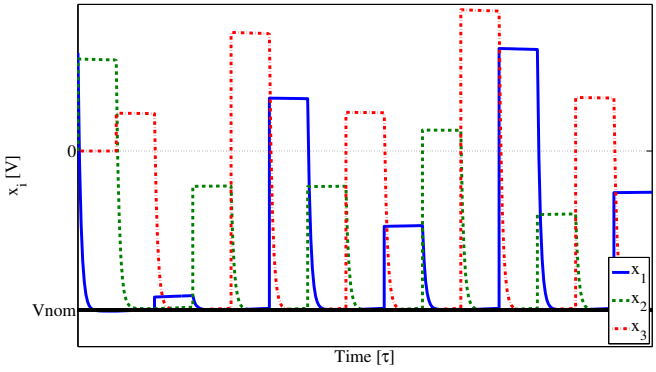

Fig. 8. Sample time history of wedge voltages with random reset.

To assess the robustness with respect to uncertainty in knowledge of wedge dynamics, i.e., uncertainty in a_1, we apply the controller (31) to a model (27) where the parameter a_1 has been perturbed from its nominal value by $+50\%$. In this case, the performance of the controller is illustrated in Fig. 7. Note that, although the steady-state output voltage is

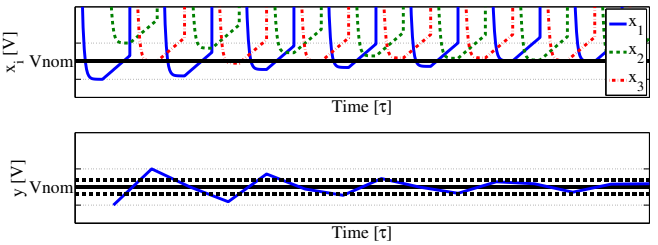

Fig. 9. Behavior of the photoreceptor with measurement noise.

biased with respect to V_{nom}, the voltage variation around that steady-state meets the controller specification.

The effect of measurement noise has also been investigated. It is easy to demonstrate a trade-off between the sensitivity and complementary sensitivity of the closed loop equations of the cyclic system. Indeed, by changing the controller gain, the variance of the wedge voltages is reduced to meet performance specifications at the expense of taking a greater number of revolutions to track V_{nom} (see Fig. 9).

IV. CONCLUSIONS AND FUTURE WORK

This paper developed an approach to the control of systems with rotating dynamics and stroboscopic instrumentation. The initial results of application to a xerographic process are reported and it is shown that time-delayed feedback ensure the required properties of stability, robustness and disturbance rejection.

The theoretical part of the future work will include development of the general theory of stabilizability, controllability and observability of cyclic systems. From the application point of view, this work will include verification of the controls using an infinite dimensional model of a cyclic system, and experimental verification using an actual xerographic product.

REFERENCES

[1] C.-L. Chen and G. T.-C. Chiu, "Banding reduction in electrophotographic processes using human contrast sensitivity function shaped photoconductor velocity control," *Journal of Imaging Science and Technology*, vol. 47, May/June 2003.

[2] D. A. Hays and K. R. Ossman, "Electrophotographic copying and printing (xerography)," in *The Optics Encyclopedia: Basic Foundation and Practical Applications*, T. G. Brown, K. Creath, H. Kogelnik, M. A. Kriss, J. Schmit, and M. J. Weber, Eds. Wiley, 2004.

[3] F. Liu, G. T. C. Chiu, E. S. Hamby, and Y. Eun, "Control analysis of a hybrid two-component development process," in *Proceedings of the IS&T NIP 22 International Conference on Digital Printing Technologies*, 2006, pp. 564–567.

[4] T. Kagawa, T. Kamimura, T. Tamura, and S. Yokota, "Fixing device having an externally-heated fixing roller," US Patent 6088549.

[5] S. Bittanti and P. Colaneri, *Periodic Systems: Filtering and Control*. Springer, 2008.

[6] T. Yang, "Impulsive control," *IEEE Transactions on Automatic Control*, vol. 44, May 1999.

[7] R. M. Gray, *Toeplitz and Circulant Matrices: A Review*. Now Publishers Inc., 2006.